

# Entanglement entropy as a probe of topological phase transitions

Manish Kumar,<sup>1</sup> Bharadwaj Vedula,<sup>1</sup> Suhas Gangadharaiah,<sup>1</sup> and Auditya Sharma<sup>1</sup>

<sup>1</sup>*Department of Physics, Indian Institute of Science Education and Research, Bhopal, Madhya Pradesh 462066, India*

(Dated: February 16, 2026)

Entanglement entropy (EE) provides a powerful probe of quantum phases, yet its role in identifying topological phase transitions in disordered systems remains underexplored. We introduce an exact EE-based framework that captures topological phase transitions even in the presence of disorder. Specifically, for a class of Su-Schrieffer-Heeger (SSH) model variants, we show that the difference in EE between half-filled and near-half-filled ground states,  $\Delta S^A$ , vanishes in the topological phase but remains finite in the trivial phase, a direct consequence of edge-state localization. This behavior persists even in the presence of quasiperiodic or binary disorder. By analyzing domain-wall configurations in the SSH chain, we further show how subsystem tuning allows one to distinguish genuine topological zero-energy eigenstates from trivial localized states. Exact phase boundaries, derived from Lyapunov exponents via transfer matrices, agree closely with numerical results from  $\Delta S^A$  and the topological invariant  $\mathcal{Q}$ , with instances where  $\Delta S^A$  outperforms  $\mathcal{Q}$ . Our results highlight EE as a robust diagnostic tool and a potential bridge between quantum information and condensed matter approaches to topological matter.

## I. INTRODUCTION

Entanglement entropy (EE) has become a central tool in the study of quantum many-body systems, and quantum phase transitions (QPTs) [1–4]. Defined as the von Neumann entropy of a subsystem, it quantifies the degree of quantum correlations between parts of a system [5]. In conventional systems, QPTs are typically associated with symmetry breaking phenomena [6–8]. However, many exotic phases such as topological insulators and fractional quantum Hall states, do not fit within this paradigm. Topological phases of matter have been an active field of research in condensed matter physics [9–14] ever since the discovery of the quantum Hall effect [15]. These phases are distinguished by topological invariants [16–21] that remain robust against local perturbations [22–25]. The far-reaching implications of these discoveries [26–29], have inspired work across fields including photonic systems [30–32], ultracold atoms [33–36], and quantum information technologies [37, 38].

Traditionally, topological phase transitions are identified using momentum-space invariants like the winding number [39, 40], and the  $\mathbb{Z}_2$  invariant [41] which rely on translational symmetry and thus break down in disordered systems. To address this, real-space alternatives, such as real space winding numbers [42] and scattering coefficients sensitive to edge-state localization [43, 44], have been developed. Among these, EE has emerged as a uniquely powerful probe. Its non-local character [45] enables detection of topological properties even in many-body states [46, 47] where conventional order parameters fail. In this work we provide an exact framework to use many body EE to study topological phase transitions which works even in the presence of disorder.

Despite many studies, a comprehensive understanding of EE across topological phase transitions remains incomplete. While EE's sensitivity to distinct topological phases is well-established [45–56], the microscopic connection between entanglement patterns and edge-state

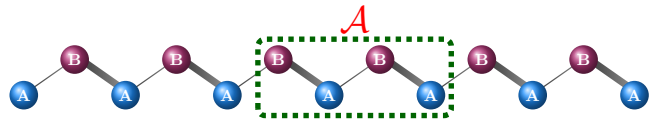


FIG. 1. SSH chain where the green dashed box shows subsystem  $\mathcal{A}$  composed of a few unit cells deep inside the bulk. In this paper, the subsystems are denoted by calligraphic letters  $\mathcal{A}$  and  $\mathcal{B}$ , while the lattice sites within each unit cell are labeled by  $A$  and  $B$ .

localization, especially in disordered systems, remains poorly understood. This gap motivates our work, where we develop a systematic framework using many particle EE to distinguish topological and trivial phases. For this purpose, we choose the Su-Schrieffer-Heeger (SSH) model [57, 58], which was first introduced to describe both elastic and electronic properties of polyacetylene, a quasi-one-dimensional polymer chain. It is a 1D tight-binding model with non-interacting spinless fermions, and is a standard test-bed for explorations on topological systems. One of the most striking features of the SSH chain is the presence of chiral symmetry protected zero-energy edge states in the topologically non-trivial phase which are robust to local perturbations that preserve the bulk gap and symmetry [59–68].

In this paper, we propose an EE based approach to study topological phase transitions and demonstrate its robustness by performing an independent transfer matrix based analysis. Specifically, we analytically derive the topological-trivial phase boundaries by calculating the Lyapunov exponent (LE) of edge states in the topological region. While this transfer-matrix-based calculation of the LE has been widely used in the studies of mobility edges in disordered systems [69–73] and Majorana fermionic systems [43, 44, 74], it has not been used in the context of the SSH model. We demonstrate that the phase boundaries obtained from the two methods match

perfectly with each other. We further use the topological quantum number  $Q$  [43] which is a well-established quantity that characterizes the presence or absence of Majorana bound states in 1D p-wave superconductors. We also show an example with disorder where EE works better than  $Q$  which exhibits some ambiguity. Finally, we present a detailed analysis of domain-wall configurations in the SSH chain to clarify the scope and interpretation of our entanglement-based diagnostic. We show that while the EE-based quantity primarily detects edge localization, combining it with a systematic tuning of the subsystem allows one to distinguish genuine topological zero-energy states from trivial localized states. This domain-wall analysis establishes a consistent framework for identifying topological phases beyond simple localization criteria.

The paper is organized as follows. Section II introduces the SSH model and its disordered variants, establishing the theoretical framework for our study. In Section III, we derive exact phase boundaries through the transfer matrix method, computing the Lyapunov exponent to distinguish topological and trivial phases. Section IV A demonstrates how the entanglement entropy difference between half-filled and half-plus-one-filled regimes serves as a robust numerical probe of the phase transition. The physical origin of this behavior is elucidated in Section IV B through occupation number analysis, revealing the edge localization of added particles in the topological phase. Section IV C addresses the scenario of topologically trivial states localized at the edges and clarifies the conditions under which our entanglement-entropy-based diagnostic distinguishes genuine topological edge states from accidental edge-localized states. Section A discusses the topological quantum number  $Q$  and its performance as a diagnostic in relation to the other measures proposed here. In Section V, we further analyze domain-wall configurations in the SSH chain and show how a systematic tuning of the subsystem enables a clear distinction between topological and non-topological localized states. Finally, Section VI summarizes our results and discusses their broader implications. Appendix B presents additional results for other parameter choices of binary disorder, demonstrating the generality of our analytical framework.

## II. MODELS

The Su–Schrieffer–Heeger (SSH) model [57, 58] describes a one-dimensional dimerized lattice with two sites per unit cell and staggered nearest-neighbour hopping. In second-quantized form the Hamiltonian is

$$H = \sum_{n=1}^L \left[ t_1 a_n^\dagger b_n + t_2 a_{n+1}^\dagger b_n + \text{H.c.} \right], \quad (1)$$

where  $a_n^\dagger$  ( $b_n^\dagger$ ) creates a particle on sublattice A (B) of the  $n^{\text{th}}$  unit cell, and  $L$  is the total number of unit cells. Since

each unit cell contains two sites, the total number of sites is  $N = 2L$ . The first term represents intracell hopping with strength  $t_1$ , whereas the second corresponds to intercell hopping with strength  $t_2$ . The competition between these two hopping parameters determines the topological phase of the system. In particular if  $|t_1| > |t_2|$  the system is in the trivial phase while for  $|t_1| < |t_2|$ , the system is in the topological phase. The edge modes in the topological phase are protected by chiral symmetry and remain stable against perturbations that preserve this symmetry and do not close the bulk energy gap. In this paper, apart from the clean SSH model, we extend the study to two disordered but chiral symmetry preserving variants of the SSH model: one in which the hopping terms are quasiperiodic and the other with binary random disorder. Our results show that the proposed analytical as well as numerical methods reliably detect topological phase transitions even in the presence of disorder, demonstrating its robustness and consistency with established results in the literature.

### A. Clean SSH model

A convenient representation of the clean SSH model is to parameterize it with average hopping amplitude  $t$ , and dimerization strength  $\lambda$ . Thus the intracell and intercell hopping terms, respectively, are given by

$$\begin{aligned} t_1 &= t - \lambda, \\ t_2 &= t + \lambda. \end{aligned} \quad (2)$$

Here we focus on the case  $t > 0$ ; the results for  $t < 0$  can be obtained analogously. When  $\lambda > 0$  the intercell hopping dominates, yielding a nonzero winding number [39, 40], and, under open boundary conditions, a pair of zero-energy edge states—signatures of a topologically non-trivial phase. For  $\lambda < 0$  the intracell hopping prevails, the winding number vanishes, and no edge states appear, so the phase is topologically trivial. Hence the relative strength of intercell and intracell hopping controls the topological character of the SSH chain.

### B. SSH model with quasiperiodic disorder hopping

Next, we introduce a quasiperiodic modulation in the hopping amplitudes of the SSH model [60, 61]. The modified intracell and intercell hopping terms, respectively, are

$$\begin{aligned} t_1 &= t - \lambda - \delta \cos(2\pi\beta n + \phi), \\ t_2 &= t + \lambda + \delta \cos(2\pi\beta n + \phi). \end{aligned} \quad (3)$$

Note that this modification leaves the chiral symmetry intact. Here we focus on the case with  $\lambda > 0$  and  $\delta > 0$ . The parameter  $\beta = (\sqrt{5} - 1)/2$  (the inverse golden ratio) ensures incommensurate modulation, preventing periodic

recurrence and thus preserving quasiperiodicity. Here,  $\phi$  is an arbitrary global phase drawn randomly from a uniform distribution in  $[0, 2\pi]$ , ensuring that the quasiperiodic potential explores all phase configurations ergodically. In previous studies, it has been conjectured that on adding this quasiperiodic potential in the hopping term, the topological phase transition occurs at  $\delta = t + \lambda$  [60]. However, an exact derivation of this phase boundary has been lacking. In this work, we analytically derive the boundary using the Lyapunov exponent of the edge state obtained via the transfer matrix method. Furthermore, we verify this analytical result numerically using the entanglement entropy. Our results show that for  $\delta < t + \lambda$  the system behaves as a topological insulator whereas for  $\delta > t + \lambda$  it is a trivial insulator.

### C. SSH model with random binary disorder hopping

We introduce random binary disorder in the hopping strength in the SSH model. To do this, we set the hopping strengths to be

$$\begin{aligned} t_1 &= t - \lambda - \Delta_n, \\ t_2 &= t + \lambda + \Delta_n. \end{aligned} \quad (4)$$

Here, the  $\Delta_n$  are drawn from a bimodal probability distribution function [62]

$$\mathcal{P}(\Delta_n) = P \delta(\Delta_n - V_0) + (1 - P) \delta(\Delta_n - W), \quad (5)$$

where  $W$  is the disorder strength and  $V_0$  is the offset, which we fix at 2. Hence,  $\Delta_n$  can take values

$$\Delta_n = \begin{cases} 2, & \text{with probability } P; \\ 2 - W, & \text{with probability } 1 - P. \end{cases} \quad (6)$$

Although random binary disorder in the hopping terms of the SSH model has been explored in earlier studies [62], the specific form considered in Eq. (4) has not been previously analyzed. In this work, we demonstrate that the LE calculated via the transfer matrix method provides a reliable analytical approach to determine the topological phase boundary. We derive the general expression for the phase boundary for an arbitrary probability  $P$ . Also, our numerical results show that entanglement entropy is also able to clearly distinguish the topological phase from the trivial phase. In this paper, we mainly focus on the case of  $P = 1/2$ . Results for  $P = 1/3$  are relegated to the Appendix B.

### III. ANALYTICAL STUDY USING TRANSFER MATRIX

We first determine the analytical expressions for the boundary of the topological-trivial phase transition by focusing on the localization properties of the zero-energy

edge modes. A good quantity to capture the localization behavior is the Lyapunov exponent  $\gamma$ , which is positive for localized states, and vanishes for delocalized states. In the topological phase, the edge modes are spatially localized on edges, yielding a positive value for LE; as we approach the phase boundary, the edge modes merge into the bulk and the LE tends to zero.

To compute  $\gamma$  for the edge modes, we employ the transfer-matrix method, allowing us to clearly identify the phase boundary between the two insulating phases. Let  $\psi_{n,A}$  and  $\psi_{n,B}$  be the wavefunction amplitudes at the  $A$  and  $B$  sites of the  $n^{\text{th}}$  unit cell, respectively. The Schrödinger equation  $H\psi = E\psi$  gives the coupled equations:

$$E\psi_{n,A} = t_1\psi_{n,B} + t_2\psi_{n-1,B}, \quad (7)$$

$$E\psi_{n,B} = t_1\psi_{n,A} + t_2\psi_{n+1,A}. \quad (8)$$

From Eq. (8), we express  $\psi_{n+1,A}$  as

$$\psi_{n+1,A} = \frac{E\psi_{n,B} - t_1\psi_{n,A}}{t_2}. \quad (9)$$

Shifting Eq. (7) by one lattice site,

$$E\psi_{n+1,A} = t_1\psi_{n+1,B} + t_2\psi_{n,B}.$$

Substituting  $\psi_{n+1,A}$  from Eq. (9) into the above gives

$$E \left( \frac{E\psi_{n,B} - t_1\psi_{n,A}}{t_2} \right) = t_1\psi_{n+1,B} + t_2\psi_{n,B}.$$

Rewriting, we obtain

$$\psi_{n+1,B} = -\frac{E}{t_2}\psi_{n,A} + \frac{E^2 - t_2^2}{t_1t_2}\psi_{n,B}. \quad (10)$$

Combining Eqs. (9) and (10), the dynamics can be expressed in the transfer-matrix form:

$$\begin{pmatrix} \psi_{n+1,A} \\ \psi_{n+1,B} \end{pmatrix} = T_n \begin{pmatrix} \psi_{n,A} \\ \psi_{n,B} \end{pmatrix}, \quad (11)$$

where the transfer matrix is

$$T_n = \begin{pmatrix} -\frac{t_1}{t_2} & \frac{E}{t_2} \\ -\frac{E}{t_2} & \frac{E^2 - t_2^2}{t_1t_2} \end{pmatrix}. \quad (12)$$

For the states at  $E = 0$ , the transfer matrix reduces to

$$T_n(E = 0) = \begin{pmatrix} -\frac{t_1}{t_2} & 0 \\ 0 & -\frac{t_2}{t_1} \end{pmatrix}. \quad (13)$$

The Lyapunov exponent associated with the zero-energy modes is defined as

$$\gamma_0 = \lim_{L \rightarrow \infty} \frac{1}{L} \ln \|\mathcal{T}_L\|, \quad (14)$$

where

$$\mathcal{T}_L = \prod_{n=1}^L T_n \quad (15)$$

is the total transfer matrix, and  $\|\mathcal{T}_L\|$  represents its norm. We take the norm to be the largest absolute eigenvalue of the transfer matrix.

### A. Clean SSH model

For the clean SSH model, the hopping terms are given by

$$\begin{aligned} t_1 &= t - \lambda, \\ t_2 &= t + \lambda. \end{aligned} \quad (16)$$

In this case, since all the transfer matrices  $T_n$  are the same, the total transfer matrix is

$$\mathcal{T}_L = \begin{pmatrix} \left(-\frac{t_1}{t_2}\right)^L & 0 \\ 0 & \left(-\frac{t_2}{t_1}\right)^L \end{pmatrix}. \quad (17)$$

Here we want to calculate the Lyapunov exponent of the edge states. For edge states to appear, the system has to be in the topological regime, i.e.  $|t_2| > |t_1|$ . Therefore, following Eqs. (14) and (15), the LE is

$$\gamma_0 = \lim_{L \rightarrow \infty} \frac{1}{L} \ln \left| \left( \frac{t_2}{t_1} \right)^L \right| = \ln \left| \frac{t_2}{t_1} \right|. \quad (18)$$

In the topological region  $\gamma_0 > 0$  because of the localized nature of the edge states and  $\gamma_0 \rightarrow 0$  as we approach the phase boundary. Hence the boundary of the topological phase is

$$\left| \frac{t_2}{t_1} \right| = 1. \quad (19)$$

Since  $t_1$  and  $t_2$  are given by Eq. (16), the topological phase boundaries become

$$\lambda = 0, \quad t = 0. \quad (20)$$

### B. Quasiperiodic disorder

In the SSH model with quasiperiodic disorder in the hopping term, the intercell and the intracell hopping are given by Eq. (3). Using equation Eq. (15), the total transfer matrix is

$$\mathcal{T}_L = \begin{pmatrix} 1/Z & 0 \\ 0 & Z \end{pmatrix}, \quad (21)$$

where

$$Z = (-1)^L \prod_{n=1}^L \frac{t + \lambda + \delta \cos(2\pi\beta n + \phi)}{t - \lambda - \delta \cos(2\pi\beta n + \phi)}. \quad (22)$$

Here  $|Z| > |1/Z|$ , the reason for which will be clear once we obtain the expression for the LE by considering  $|Z|$  as the norm of the transfer matrix. From Eqs. (14) and (15) the LE of the edge states is

$$\gamma_0 = \lim_{L \rightarrow \infty} \frac{1}{L} \ln |Z|, \quad (23a)$$

$$= \lim_{L \rightarrow \infty} \frac{1}{L} \ln \left| \prod_{n=1}^L \frac{t + \lambda + \delta \cos(2\pi\beta n + \phi)}{t - \lambda - \delta \cos(2\pi\beta n + \phi)} \right|. \quad (23b)$$

Since  $\beta$  is an irrational number, as  $n$  varies, the interval  $[0, 2\pi]$  fills uniformly. This follows from Weyl's equidistribution theorem and properties of irrational rotations [75, 76]. Then by using the classical Jensen's formula [77, 78], we can write

$$\begin{aligned} \gamma_0 &= \frac{1}{2\pi} \int_0^{2\pi} \ln \left| \frac{t + \lambda + \delta \cos \theta}{t - \lambda - \delta \cos \theta} \right| d\theta \\ &= \frac{1}{2\pi} \int_0^{2\pi} \ln |t + \lambda + \delta \cos \theta| d\theta \\ &\quad - \frac{1}{2\pi} \int_0^{2\pi} \ln |t - \lambda - \delta \cos \theta| d\theta. \end{aligned}$$

Both integrals are of the form

$$\frac{1}{2\pi} \int_0^{2\pi} \ln |a + b \cos u| du = \begin{cases} \ln \frac{|a| + \sqrt{a^2 - b^2}}{2}, & \text{if } |a| > |b|, \\ \ln \frac{|b|}{2}, & \text{if } |a| < |b|. \end{cases}$$

Using this expression and a careful analysis of the inequalities, the Lyapunov exponent  $\gamma_0$  for the edge state can be written as

$$\gamma_0 = \begin{cases} \ln \frac{t + \lambda + \sqrt{(t + \lambda)^2 - \delta^2}}{|t - \lambda| + \sqrt{(t - \lambda)^2 - \delta^2}}, & \text{if } \delta < |t - \lambda|, \\ \ln \frac{t + \lambda + \sqrt{(t + \lambda)^2 - \delta^2}}{\delta}, & \text{if } |t - \lambda| < \delta < t + \lambda. \end{cases} \quad (24)$$

Clearly,  $\gamma_0 > 0$  for  $\delta < t + \lambda$ , indicating localized edge states and hence a topological insulating phase. In contrast,  $\gamma_0 \rightarrow 0$  as  $\delta \rightarrow t + \lambda$ , therefore the topological phase boundary is

$$\delta = t + \lambda. \quad (25)$$

This analytical expression is consistent with both our numerical results and earlier numerical studies on the SSH model with quasiperiodic modulation in the hopping amplitudes [60].

From Eq. (21) we can see that the total transfer matrix  $\mathcal{T}_L$  has two eigenvalues  $Z$  and  $1/Z$ . The LE obtained in

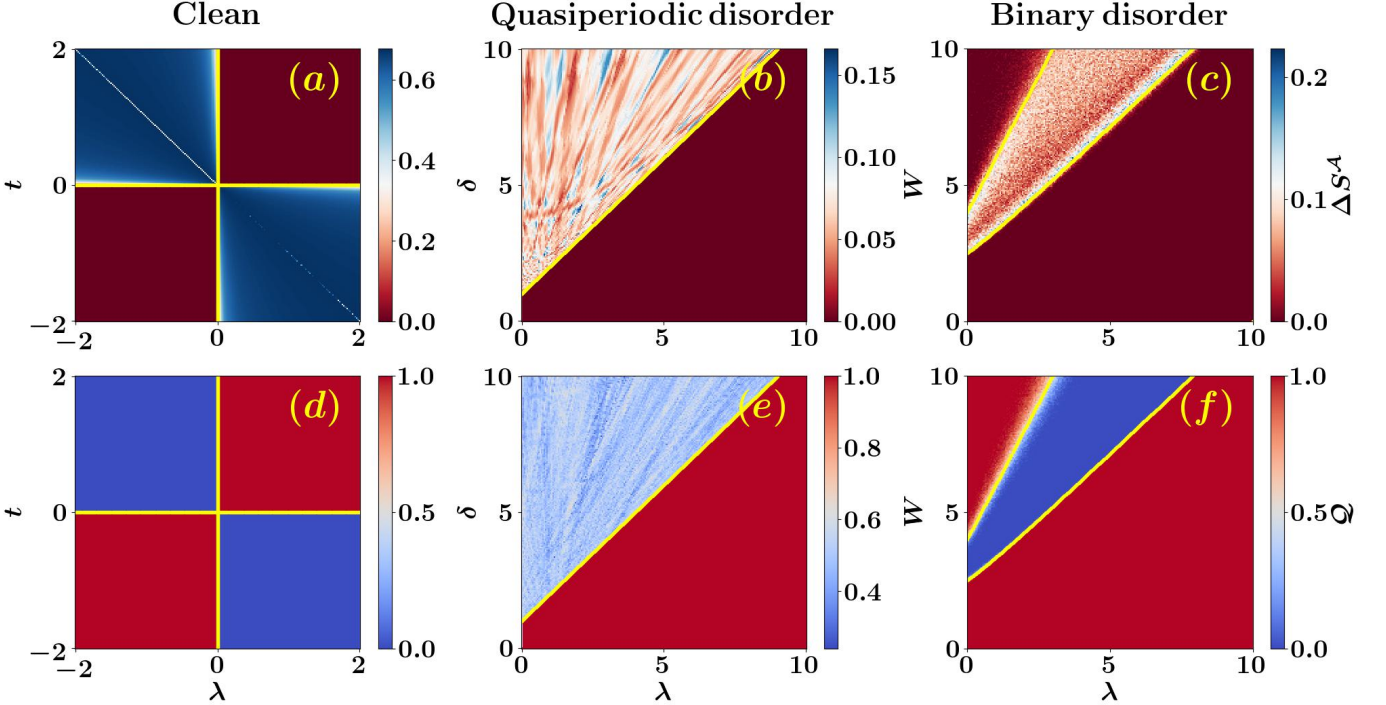


FIG. 2. Phase diagrams of the SSH model variants. In (a)–(c) the color scale denotes  $\Delta S^A = |S_{\text{hf}}^A - S_{\text{hf}+1}^A|$  with  $\text{hf} = N/2$ , and the subsystem size  $N_A = 50$ . In (d)–(f) the color scale denotes topological quantum number  $Q$ , which is defined in Appendix A. For the disordered cases with  $t = 1$ , the results shown are averaged over 100 disorder realizations. For all the figures, system size  $N = 400$ . Yellow curves mark analytical phase boundaries. On the diagonal line  $t = -\lambda$  in (a), the intracell hopping vanishes, causing the system to break into disconnected segments. Therefore the state just above half filling becomes localized on a few sites, reducing its contribution to the entanglement entropy and hence yielding a smaller  $\Delta S^A$ .

Eq. (24) is by considering the eigenvalue  $Z$ . Hence, a positive value of  $\gamma_0$  indicates that  $|Z| > 1$  (according to Eq. (23a)), supporting our choice of  $Z$  as the largest absolute eigenvalue.

### C. Random binary disorder

We consider the disordered SSH model where the hopping terms are given by Eq. (4) and the hopping modulation  $\Delta_n$  is given by Eq. (6). Here,  $\Delta_n$  can take only two values for any  $n$ , and hence the transfer matrices can take only two possible forms,

$$T_a = \begin{pmatrix} -v & 0 \\ -u & -u \\ 0 & -u \\ 0 & v \end{pmatrix} \quad (26)$$

corresponding to  $\Delta_n = 2$  (with probability  $P$ ), and

$$T_b = \begin{pmatrix} -v + W & 0 \\ -u - W & -u - W \\ 0 & -u - W \\ 0 & v + W \end{pmatrix} \quad (27)$$

corresponding to  $\Delta_n = 2 - W$  (with probability  $1 - P$ ), where  $u = t + \lambda + 2$  and  $v = t - \lambda - 2$ . Hence, in Eq. (15) for the total transfer matrix,  $T_a$  appears  $PL$  number of

times, and  $T_b$  appears  $(1 - P)L$  number of times in the product. Furthermore, since the transfer matrices  $T_a$  and  $T_b$  commute in our case, the total transfer matrix can be written as

$$\mathcal{T}_L = T_a^{LP} T_b^{L(1-P)}. \quad (28)$$

Using Eqs. (14) and (15) the LE of the edge states can be written as

$$\gamma_0 = P \ln \|T_a\| + (1 - P) \ln \|T_b\|. \quad (29)$$

For the edge modes to exist, the intercell hopping has to be larger than the intracell hopping, i.e.,  $|t_2| > |t_1|$ . Therefore,  $\|T_a\| = \left| \frac{u}{v} \right|$  and  $\|T_b\| = \left| \frac{u - W}{v + W} \right|$ . Hence,

$$\begin{aligned} \gamma_0 &= P \ln \left| \frac{u}{v} \right| + (1 - P) \ln \left| \frac{u - W}{v + W} \right| \\ &= \ln \left( \left| \frac{u}{v} \right|^P \left| \frac{u - W}{v + W} \right|^{1-P} \right) \\ &= \ln \left| \left( \frac{u}{v} \right)^P \left( \frac{u - W}{v + W} \right)^{1-P} \right|. \end{aligned} \quad (30)$$

The phase transition occurs when  $\gamma_0 = 0$ , thus

$$\left| \left( \frac{u}{v} \right)^P \cdot \left( \frac{u - W}{v + W} \right)^{1-P} \right| = 1. \quad (31)$$

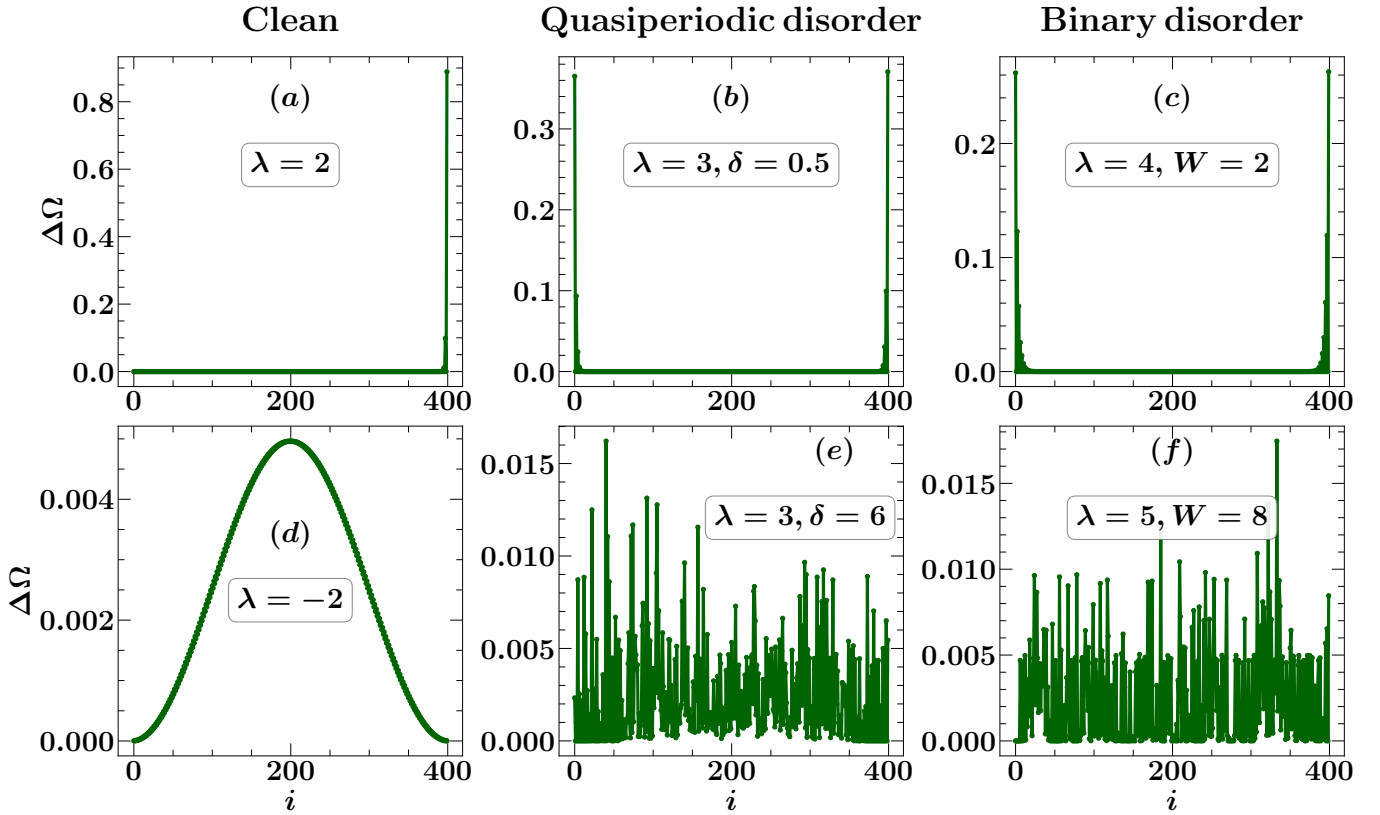


FIG. 3. Spatial distribution of  $\Delta\Omega = |\Omega_{\text{hf}} - \Omega_{\text{hf+1}}|$  for a system of size  $N = 400$  at half-filling ( $\text{hf} = 200$ ). The hopping amplitude is  $t = 1$  for all cases. Subfigures (a)–(c) correspond to the topological phase, while (d)–(f) correspond to the trivial phase.

Note that  $u > 0$  for  $t, \lambda > 0$ . However,  $v$  can be negative as well as positive. For  $v > 0$ ,

$$W_{\pm} = \frac{u^{\frac{1}{1-P}} \mp v^{\frac{1}{1-P}}}{u^{\frac{P}{1-P}} \pm v^{\frac{P}{1-P}}}, \quad (32)$$

and for  $v < 0$ ,

$$W_{\pm} = \frac{u^{\frac{1}{1-P}} \mp (-v)^{\frac{1}{1-P}}}{u^{\frac{P}{1-P}} \mp (-v)^{\frac{P}{1-P}}}. \quad (33)$$

These equations yield the boundaries separating the topological insulator phase from the trivial insulator phase. We confirm these boundaries, with a numerical study for  $P = 1/2$  in the next section and for  $P = 1/3$  in the Appendix B.

#### IV. ENTANGLEMENT ENTROPY BASED DIAGNOSTIC FOR EDGE LOCALIZATION

In this section, we investigate the phase transition between topological and trivial insulating states using the entanglement entropy as a diagnostic measure. We demonstrate that the entanglement entropy is an effective quantity for distinguishing between these two phases.

To gain further insight into the behavior of the entanglement entropy, we analyze the occupation numbers of the full system. We contrast our results against those of the topological invariant  $\mathcal{Q}$  in Appendix A. We briefly review these quantities and present our results.

##### A. Entanglement Entropy

Entanglement entropy (EE) is a quantity used to measure entanglement in a pure state of a bipartite system. In general, to calculate EE, one uses the reduced density matrix approach. In this approach, we first partition the entire system appropriately into subsystems  $\mathcal{A}$  and  $\mathcal{B}$ . The entanglement entropy of the subsystem  $\mathcal{A}$  can then be written as  $S^{\mathcal{A}} = -\text{Tr}(\rho_{\mathcal{A}} \log \rho_{\mathcal{A}})$ , where  $\rho_{\mathcal{A}} = \text{Tr}_{\mathcal{B}}(\rho)$  is the reduced density matrix of subsystem  $\mathcal{A}$  obtained by tracing out the degrees of freedom of the subsystem  $\mathcal{B}$  from the overall state  $\rho$ . In our work, we study the EE of the many-body ground state  $\rho = |\Psi_0\rangle\langle\Psi_0|$ . To obtain this using exact diagonalization, we first have to diagonalize the Hamiltonian (which is a  $2^N \times 2^N$  matrix, with  $N = 2L$  being the total number of sites) to find the ground state  $|\Psi_0\rangle$ , and then computing  $S^{\mathcal{A}}$  involves diagonalizing  $\rho_{\mathcal{A}}$ .

For free fermionic systems, Peschel et. al. [79–81] de-

veloped an approach, the correlation matrix approach, that drastically reduces the computation time. The details of the method are as follows. For non-interacting fermionic systems, since the ground state has the structure of a Slater determinant, Wick's theorem can be exploited to express the reduced density matrix in the form  $\rho_{\mathcal{A}} = e^{-H_{\mathcal{A}}}/Z$ , where  $H_{\mathcal{A}}$  is the entanglement Hamiltonian and  $Z$  is a normalization factor ensuring  $\text{Tr}(\rho_{\mathcal{A}}) = 1$ . The correlation matrix  $C$  for the full system is defined as  $C_{ij} = \langle c_i^\dagger c_j \rangle$  and has dimension  $N \times N$ . Subsequently, one selectively extracts the portion of the correlation matrix that pertains to the subsystem of interest and the correlation matrix of the subsystem  $\mathcal{A}$ , i.e.  $C^{\mathcal{A}}$  becomes of the order of  $L \times L$ . The correlation matrix,  $C^{\mathcal{A}}$  and the entanglement Hamiltonian  $H_{\mathcal{A}}$  are related as [79–81]

$$C^{\mathcal{A}} = \frac{1}{e^{H_{\mathcal{A}}} + 1}. \quad (34)$$

The entanglement entropy between the subsystems  $\mathcal{A}$  and  $\mathcal{B}$  for free fermions is determined using eigenvalues  $\lambda_k$  of the subsystem correlation matrix by [80, 81]

$$S^{\mathcal{A}} = - \sum_k [\lambda_k \ln \lambda_k + (1 - \lambda_k) \ln(1 - \lambda_k)]. \quad (35)$$

This method provides an efficient way to compute the entanglement entropy of the many particle ground state of free fermions and has been extensively used in recent works for various models.

We demonstrate that the EE of the many-body ground state is an effective probe of the quantum phase transition between the topological and trivial (band) insulating phases. We compute the difference in EE between the many-particle ground state at half-filling and the state with one more than half filling, defined as

$$\Delta S^{\mathcal{A}} = |S_{\text{hf}}^{\mathcal{A}} - S_{\text{hf+1}}^{\mathcal{A}}|. \quad (36)$$

To utilize EE as a diagnostic measure, it is crucial to define the subsystem appropriately. We find that choosing a subsystem  $\mathcal{A}$  consisting of a few unit cells deep within the bulk as shown in the schematic (Fig. 1), and the remaining sites as subsystem  $\mathcal{B}$ , is an effective choice. The rationale for this choice will become clear in the subsequent analysis. We note that considering the difference with respect to a state with one particle fewer than half-filling ( $|S_{\text{hf}}^{\mathcal{A}} - S_{\text{hf-1}}^{\mathcal{A}}|$ ) also yields the same qualitative behavior across the phase transition. Here we focus on the results for one particle added beyond half-filling.

As discussed earlier, the clean SSH model (Eq. (16)), exhibits a topological phase transition from a trivial to a topological insulator, depending on the relative strengths of intercell and intracell hopping amplitudes. We plot the phase diagram of  $t$  and  $\lambda$  with  $\Delta S^{\mathcal{A}}$  in Fig. 2(a). In the topological region, we find  $\Delta S^{\mathcal{A}} = 0$ , implying that the EE of the half-filled ground state is identical to that of the ground state with one additional particle. In contrast, within the trivial phase,  $\Delta S^{\mathcal{A}} \neq 0$ , providing

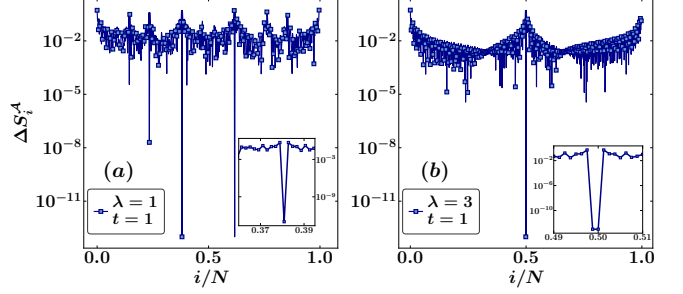


FIG. 4. Entanglement-entropy difference  $\Delta S_i^{\mathcal{A}} = |S_i^{\mathcal{A}} - S_{i+1}^{\mathcal{A}}|$  for all eigenstates in (a) the AAH model and (b) the clean SSH model. In (a), the inset shows that only a single eigenstate exhibits vanishing  $\Delta S_i^{\mathcal{A}}$ , whereas in (b), the SSH model features pairs of states with  $\Delta S_i^{\mathcal{A}} = 0$ , consistent with its topological edge modes.

a clear distinction from the topological phase. We further test our quantity  $\Delta S^{\mathcal{A}}$  for the SSH model with the quasiperiodic disorder in the hopping strength (Eq. (3)). The boundary separating the topological phase from the trivial phase is  $\delta = t + \lambda$ . The quantity  $\Delta S^{\mathcal{A}}$  can clearly distinguish two phases even for the quasiperiodic model as can be seen in Fig. 2(b). To further confirm that  $\Delta S^{\mathcal{A}}$  effectively identifies the phase transition, we check this on the SSH model with random binary disorder in hopping strength (Eq. (6)) for  $P = 1/2$ . The expression for the phase transition boundary for this case can be obtained by putting  $P = 1/2$  in Eq. (32) and Eq. (33). We plot the phase diagram for  $t = 1$  and our numerical results are in exact agreement with the analytical expression as shown in Fig. 2(c). This confirms that our quantity  $\Delta S^{\mathcal{A}}$  successfully identifies both the boundaries of the topological regions, in agreement with the analytical results. It is zero in the topological phase and nonzero in the trivial phase. We also show that this method is robust by considering other parameter values in the Appendix B. Also in section IV C, we discuss how our diagnostic fares for topologically trivial states localized at the edges.

## B. Occupation number

In the topological regime,  $\Delta S^{\mathcal{A}} = 0$  indicates that the additional particle introduced beyond half-filling does not contribute to the entanglement entropy of the subsystem  $\mathcal{A}$ . To investigate this further, we examine the spatial distribution of the added particle by analyzing the site occupations of the full system. These site occupations correspond to the diagonal elements of the full system's correlation matrix,  $C$ . In particular, we consider the change in site occupations defined as

$$\Delta\Omega = |\Omega_{\text{hf}} - \Omega_{\text{hf+1}}|, \quad (37)$$

where  $\Omega$  denotes the set of site occupations, corresponding to the diagonal elements of the full system's correlation matrix. In this way, we obtain direct information

about the location of the additional particle introduced beyond half-filling.

We study the spatial distribution of  $\Delta\Omega$  across the full system for the clean SSH model in Fig. 3(a, d), the quasiperiodic disorder case in Fig. 3(b, e), and the random binary disorder case in Fig. 3(c, f). From Figs. 3(a-c) it can be observed that in the topological phase,  $\Delta\Omega$  is nonzero only at the edges, indicating that the additional particle introduced beyond half-filling is localized exclusively at the boundaries. As a result, it does not occupy sites within subsystem  $\mathcal{A}$  and there is no change in the eigenvalues of the correlation matrix of subsystem  $\mathcal{A}$ , consequently, does not contribute to the entanglement entropy. In contrast, in the trivial phase, the added particle occupies the sites in both the subsystems  $\mathcal{A}$  and  $\mathcal{B}$ , as seen in Figs. 3(d-f), leading to a change in the eigenvalues of  $C_{\mathcal{A}}$  and hence finite contribution to the entanglement entropy, consequently leading to a nonzero value of  $\Delta S^{\mathcal{A}}$ . In all the three cases also, the additional particle is localized at the edges in the topological regime, while in the trivial regime it occupies both the edges and the bulk, yielding consistent behavior irrespective of the presence and nature of the disorder.

### C. Non-topological localized edge states away from half-filling

We discuss the possibility of observing states localized at the edges that are not of topological origin. For this purpose, we consider the Aubry–André–Harper (AAH) model, a topologically trivial system that undergoes a transition from a fully extended phase to a fully localized phase as the strength of the quasiperiodic potential is increased [82]. The model Hamiltonian is

$$H = -J \sum_{n=1}^L (c_n^\dagger c_{n+1} + \text{H.c.}) + \sum_{n=1}^L V_n c_n^\dagger c_n,$$

where  $V_n = \lambda \cos[2\pi(\beta n + \theta)]$  and  $\lambda$  is the potential strength. In this model, all eigenstates are delocalized for  $\lambda < 2t$ , whereas they become localized for  $\lambda > 2t$ . It has been observed that even in the delocalized regime, one occasionally finds eigenstates that appear localized [83]. Looking at their wavefunction profile we observe that these states are localized at the edges despite the system being topologically trivial.

We analyse these states using our entanglement entropy based quantity for the entire spectrum. We compute

$$\Delta S_i^{\mathcal{A}} = |S_i^{\mathcal{A}} - S_{i+1}^{\mathcal{A}}|,$$

where  $i$  labels the filling across the entire spectrum and  $\mathcal{A}$  is the subsystem consisting of a few unit cells deep inside the bulk. For the AAH model, we find that  $\Delta S_i^{\mathcal{A}}$  indeed vanishes for those eigenstates that are localized at the edges [Fig. 4(a)]. However, these states are not

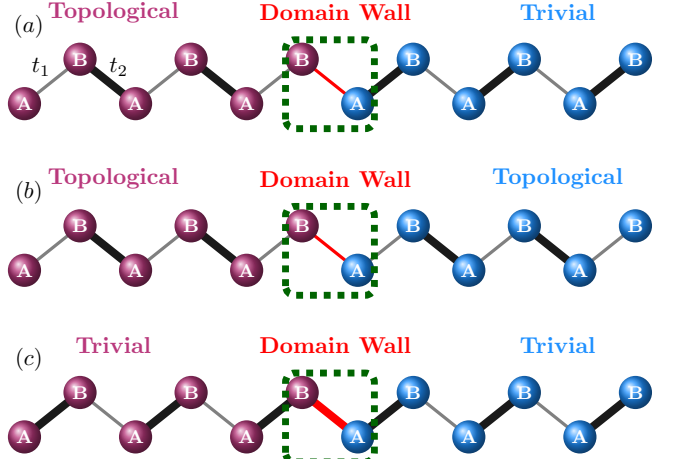


FIG. 5. Schematic illustration of situations in which domain walls arise in the SSH chain: (a) a topological SSH chain joined to a trivial SSH chain by a weak bond; (b) two topological SSH chains joined by a weak bond; and (c) two topologically trivial SSH chains joined by a strong bond.

topological as for a state to be topologically protected, it must appear at half-filling at zero energy, which is the requirement of chiral symmetry. In contrast, in the SSH model, not only states with vanishing  $\Delta S^{\mathcal{A}}$  come at half filling but also come in pairs i.e.,  $\Delta S_i^{\mathcal{A}}$  as well as  $\Delta S_{i+1}^{\mathcal{A}}$  both are zero [Fig. 4(b)], consistent with their genuine topological origin. For AAH model, states with vanishing  $\Delta S^{\mathcal{A}}$  do not come in pairs, i.e.  $\Delta S_{i+1}^{\mathcal{A}} \neq 0$ . This discussion shows that the diagnostic we propose primarily identifies edge-localized states. To use it to characterize a topological phase transition, one also has to consider the physical context.

There exist accidental situations where states localized at the edges of a system appear in pairs at  $E = 0$  and at half filling without having a topological origin, for example in superconducting wires hosting Majorana modes. Although we do not encounter such states in our present models, they can arise in the superconducting wires. However, these edge-localized states are not robust against changes in system parameters: modifying the parameters typically leads these edge states to merge with the bulk. This behavior can be exploited by altering the length of the topological region in a superconducting wire. If the edge states have a genuine topological origin, and the few sites are tuned to be away from the topological origin, then the edge states should still survive at the new topological boundary with  $E = 0$ , and hence  $\Delta S^{\mathcal{A}}$  continues to vanish for them. On the other hand, spurious zero-energy edge states split and merge into the bulk under such modifications, resulting in a nonzero  $\Delta S^{\mathcal{A}}$ . This protocol has been discussed in detail in the context of Majorana edge modes [84], although no entanglement based measures are studied here.

There exists another class of configurations in which non-topological domain-wall states emerge near half fill-

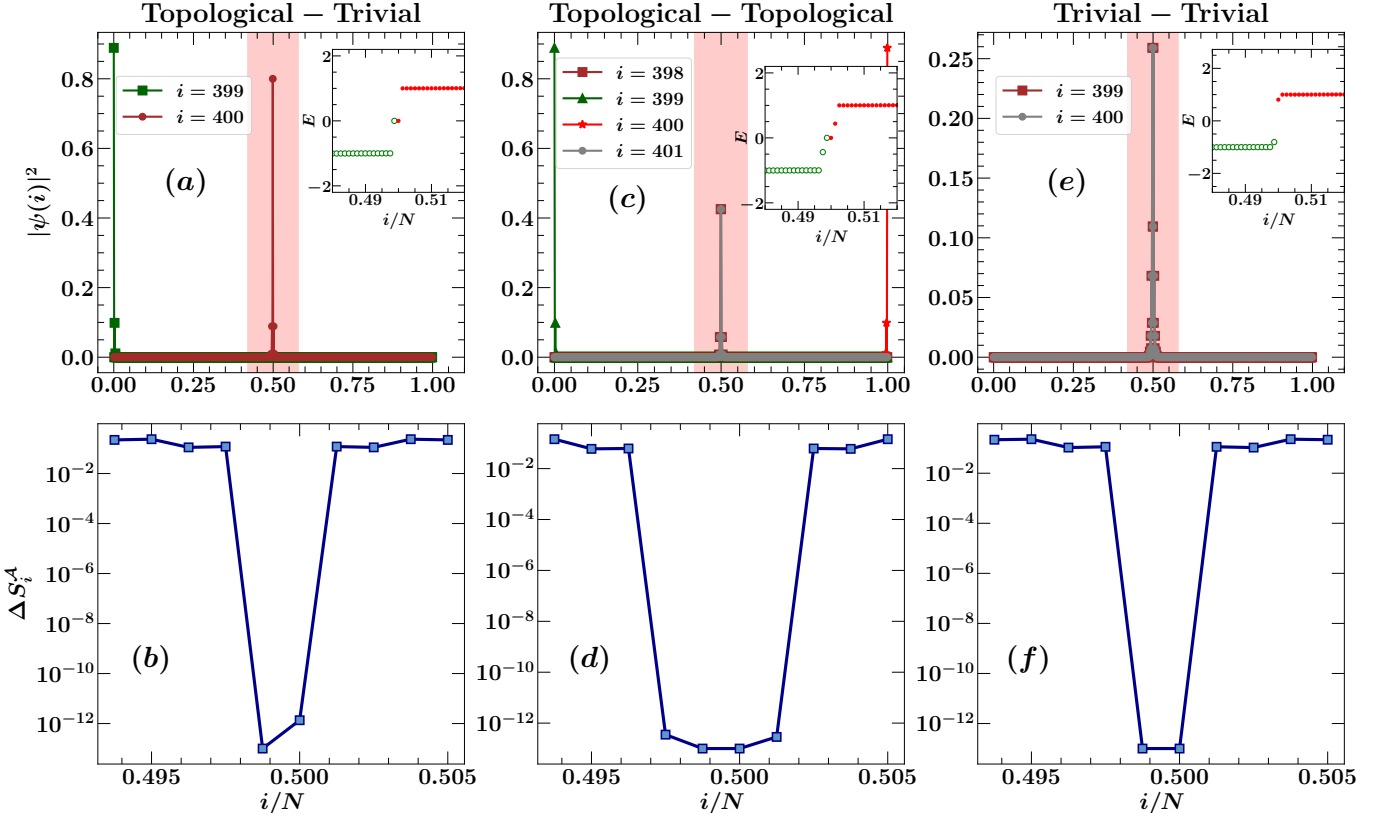


FIG. 6. Trivial-topological, topological-topological, and trivial-trivial junctions in the SSH chain. (a,c,e) Probability density  $|\psi(i)|^2$  of localized states for (a) a trivial-topological junction, (c) a topological-topological junction, and (e) a trivial-trivial junction. In panel (a), one zero-energy state is localized at the left edge and another at the domain wall. In panel (c), four localized states appear: two zero-energy edge states and two finite-energy states localized at the domain wall. In panel (e), two finite-energy states are localized at the domain wall. The red shaded region denotes subsystem  $\mathcal{A}$  with  $N_{\mathcal{A}} = 128$ , and the insets show the central part of the energy spectra. (b,d,f) Corresponding entanglement entropy difference  $\Delta S_i^A = |S_i^A - S_{i+1}^A|$  as a function of filling near half filling for the respective junctions. The vanishing values of  $\Delta S_i^A$  correspond to the localized states shown in the upper panels. For topological SSH chain  $t_1 = 0.5$  and  $t_2 = 1.5$ , and for the trivial SSH chain  $t_1 = 1.5$  and  $t_2 = 0.5$ . The system size is  $N = 800$  in all the figures.

ing. In the following section, we analyze this case in detail and outline a systematic approach to distinguish these trivial states from genuinely topological domain-wall states.

## V. DOMAIN-WALL STATES: DISTINGUISHING TOPOLOGICAL FROM TRIVIAL LOCALIZATION

Up to this point, the diagnostic we propose has relied on the localization properties of edge states: by detecting states localized near the system boundaries close to half filling, we identify regimes with topological character. However, there exist situations in which localized states appear near half filling without having a topological origin. The domain-wall states of the SSH chain are a striking example of this kind. In these situations, an additional level of analysis is required to correctly identify the phase.

### A. Domain-Wall States in the SSH Chain

Depending on how two SSH chains are joined, different types of domain walls may arise, as illustrated schematically in Fig. 5. When a topological SSH chain is connected to a trivial SSH chain by a weak bond [Fig. 5(a)], two zero-energy states appear: one localized at the left edge of the system and the other localized at the domain-wall position [Fig. 6(a)] [85]. When using  $\Delta S_i^A$  as a diagnostic, we choose the subsystem  $\mathcal{A}$  according to our prescription, such that the additional particle occupies only one of the two subsystems. This can be achieved by selecting  $\mathcal{A}$  so that the domain wall lies entirely either inside or outside the chosen subsystem. With this choice, the vanishing contributions to  $\Delta S_i^A$ , when evaluated near half filling, occur in pairs and correspond to the genuine topological edge states, as shown in Fig. 6(b).

We next analyze junctions formed by topological-topological and trivial-trivial SSH chains. When two topological SSH chains are connected by a weak bond

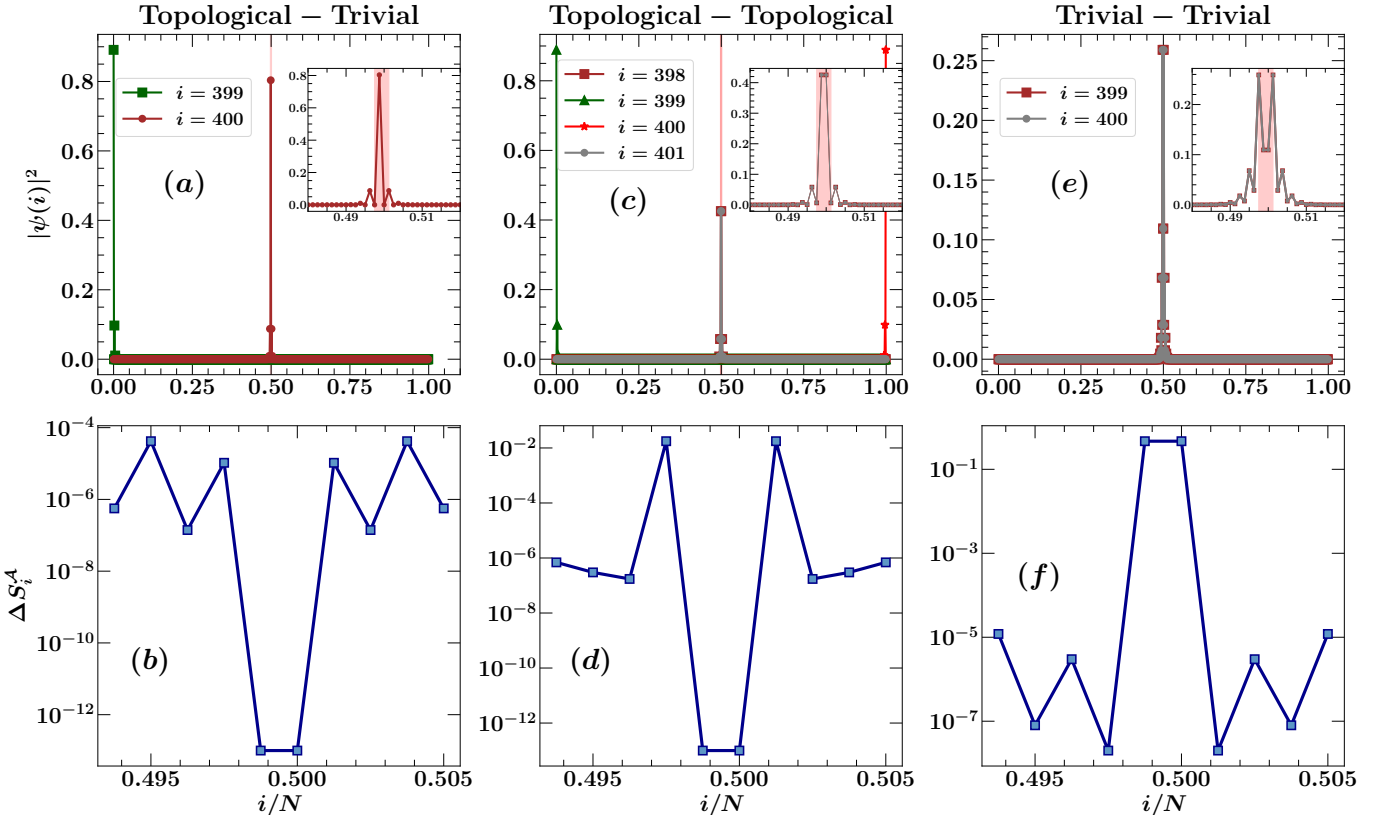


FIG. 7. Same as Fig. 6, but with subsystem  $\mathcal{A}$  chosen as  $N_{\mathcal{A}} = 4$ . The red shaded region denotes the modified subsystem, and the insets show a zoomed-in view highlighting the subsystem choice. All other parameters are identical to those in Fig. 6.

[Fig. 5(b)], in addition to the two zero-energy topological edge states, two finite-energy states localized at the domain wall appear [Fig. 6(c)], which do not have a topological origin. The corresponding entanglement entropy difference  $\Delta S_i^A$ , evaluated near half filling, exhibits four dips [Fig. 6(d)], reflecting the localized nature of these states and potentially indicating a topological signal when the subsystem is chosen according to the above prescription. Similarly, when two trivial SSH chains are connected by a strong bond [Fig. 5(c)], two finite-energy, topologically trivial states localized at the domain wall appear [Fig. 6(e)]. In this case as well,  $\Delta S_i^A$  displays two dips near half filling [Fig. 6(f)], since the added particle predominantly occupies a single subsystem. In both cases,  $\Delta S_i^A = 0$  for domain-wall states without topological origin, for the same reason discussed earlier: the added particle resides within a single chosen subsystem.

## B. Subsystem Tuning as a Topological Discriminator

In such scenarios, confirming the topological nature of the phase requires an additional step beyond the mere detection of edge localization near half-filling. This is achieved by tuning the chosen subsystem. The red shaded region in Fig. 6 indicates the initially selected

subsystem  $\mathcal{A}$ . To test the robustness of the diagnostic, we shrink the subsystem  $\mathcal{A}$  such that the particle associated with the domain-wall state has nonzero occupation in both subsystems, as illustrated in the insets of Figs. 7(a), 7(c), and 7(e). For genuine topological zero-energy states,  $\Delta S_i^A$  remains vanishing even under this modified choice of subsystem [Fig. 7(b)]. In contrast, for this choice of subsystem, no dip appears in  $\Delta S_i^A$  for non-topological finite-energy domain-wall states [Figs. 7(d) and 7(f)]. A comparison between Figs. 6 and 7 further shows that partially enveloping the domain wall reduces the number of dips in  $\Delta S_i^A$  only for non-topological domain-wall states. This demonstrates that the proposed diagnostic can distinguish zero-energy topological states from finite-energy trivial ones, even when both are spatially localized. To further understand this behavior, we examine how  $\Delta S_{\text{DW}}^A = |S_{\text{DW}}^A - S_{\text{DW}-1}^A|$ , corresponding to the case where the added particle occupies the domain-wall state, evolves as the subsystem size is reduced. As shown in Fig. 8, for a topological-trivial junction, where the domain-wall state is topological and pinned at  $E = 0$ ,  $\Delta S_{\text{DW}}^A$  remains zero upon decreasing the subsystem size. In contrast, for a trivial-trivial junction, where the domain-wall state has finite energy,  $\Delta S_{\text{DW}}^A$  increases and becomes finite as the subsystem is shrunk.

To understand the origin of this behavior, we analyze

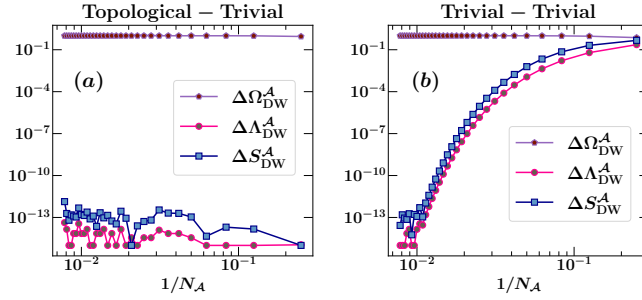


FIG. 8. Behavior of different quantities as the subsystem size  $N_{\mathcal{A}}$  is varied for domain-wall states. The horizontal axis shows  $1/N_{\mathcal{A}}$ , so moving to the right corresponds to shrinking the subsystem. Figure (a) shows a topological domain wall in a topological–trivial junction, while figure (b) shows a trivial domain wall in a trivial–trivial junction. The plotted quantities are the change in entanglement entropy  $\Delta S_{\text{DW}}^{\mathcal{A}}$ , the change in the spectral measure  $\Delta \Lambda_{\text{DW}}^{\mathcal{A}}$ , and the change in subsystem occupation  $\Delta \Omega_{\text{DW}}^{\mathcal{A}}$  when a particle is added to the domain-wall state. In the topological case (a),  $\Delta S_{\text{DW}}^{\mathcal{A}}$  remains essentially zero as the subsystem is reduced, indicating robustness of the topological state. In contrast, for the trivial case (b),  $\Delta S_{\text{DW}}^{\mathcal{A}}$  increases and becomes finite as the subsystem shrinks. The occupation change  $\Delta \Omega_{\text{DW}}^{\mathcal{A}}$  remains nearly constant in both cases. For the topological SSH chain  $t_1 = 0.5$ ,  $t_2 = 1.5$ ; for the trivial SSH chain  $t_1 = 1.5$ ,  $t_2 = 0.5$ . The system size is  $N = 800$ , and the initial subsystem size is  $N_{\mathcal{A}} = 128$ .

the changes in the eigenvalues of the subsystem correlation matrix  $C_{\mathcal{A}}$ . From Eq. (35), the contribution to the entanglement entropy from each eigenvalue vanishes when  $\lambda_k = 0$  or  $1$ , and is maximal at  $\lambda_k = 0.5$ . The change in entanglement entropy upon adding a particle can therefore be understood by tracking the redistribution of eigenvalues relative to  $0.5$ . We define

$$\Lambda_i^{\mathcal{A}} = \sum_k \left| \lambda_k - \frac{1}{2} \right|, \quad (38)$$

which measures the distribution of  $\lambda_k$ s relative to  $0.5$ , where  $i$  denotes the filling. We further define  $\Delta \Lambda_i^{\mathcal{A}} = |\Lambda_i^{\mathcal{A}} - \Lambda_{\text{DW}+1}^{\mathcal{A}}|$ . A vanishing  $\Delta \Lambda^{\mathcal{A}}$  may arise either when the eigenvalues remain unchanged or when they shift symmetrically about  $0.5$ . To contrast this spectral measure with an occupation-based quantity, we also consider  $\Omega_i^{\mathcal{A}} = \sum_k \lambda_k$ , which represents the total occupation of subsystem  $\mathcal{A}$ . We further define  $\Delta \Omega_{\text{DW}}^{\mathcal{A}} = |\Omega_{\text{DW}}^{\mathcal{A}} - \Omega_{\text{DW}+1}^{\mathcal{A}}|$ , which quantifies the fraction of the added particle entering subsystem  $\mathcal{A}$ .

We compute  $\Delta \Omega_{\text{DW}}^{\mathcal{A}}$  and  $\Delta \Lambda_{\text{DW}}^{\mathcal{A}}$  as functions of subsystem size in Fig. 8 and compare them with  $\Delta S_{\text{DW}}^{\mathcal{A}}$  as  $N_{\mathcal{A}}$  is reduced. In both Figs. 8(a) and 8(b),  $\Delta \Omega_{\text{DW}}^{\mathcal{A}}$  remains nearly unchanged upon decreasing  $N_{\mathcal{A}}$ , indicating that the fraction of the added particle residing in subsystem  $\mathcal{A}$  is similar for both topological and trivial domain-wall states. This shows that the occupation fraction alone cannot account for the distinct behavior of  $\Delta S_{\text{DW}}^{\mathcal{A}}$ . In contrast,  $\Delta \Lambda_{\text{DW}}^{\mathcal{A}}$  remains zero [Fig. 8(a)] for

the topological domain wall as  $N_{\mathcal{A}}$  decreases, whereas it becomes finite for the trivial case [Fig. 8(b)]. In fact the graph of  $\Delta \Lambda_{\text{DW}}^{\mathcal{A}}$  closely mimics that of  $\Delta S_{\text{DW}}^{\mathcal{A}}$  as shown in Fig. 8(b). We note that  $\Delta S_{\text{DW}}^{\mathcal{A}}$  remains zero as the subsystem size is shrunk although  $\Delta \Omega_{\text{DW}}^{\mathcal{A}}$  remains unchanged. This indicates that  $\Delta S_{\text{DW}}^{\mathcal{A}}$  remaining zero as the subsystem size is shrunk is not just a consequence of the topological state having very tiny localization length. In contrast to the cases described in the previous section, the added particle induces non-trivial changes in the eigenvalues of the subsystem correlation matrix. However, in the topological configuration, the redistribution of eigenvalues is symmetric around  $0.5$ , leading to  $\Delta S_{\text{DW}}^{\mathcal{A}} \approx 0$ . Thus we observe that a characteristic feature of topological domain wall states is that  $\Delta S_{\text{DW}}^{\mathcal{A}}$  remains zero as the subsystem is shrunk.

## VI. SUMMARY AND OUTLOOK

In this work, we have demonstrated that entanglement entropy (EE) can serve as an effective probe for detecting topological phase transitions in the Su-Schrieffer-Heeger (SSH) model and its disordered variants. We study the clean SSH model as well as two extensions incorporating quasiperiodic and random binary disorder in the hopping terms. We show that the entanglement entropy of the many-body ground state at half-filling, one particle above, and one particle below half-filling remains identical in the topological regime, while it differs in the trivial regime. This behaviour of EE can be understood by studying the occupation number of the sites of the full system, which reveals that the extra particle after half filling occupies the edge sites and hence does not contribute to the entanglement entropy of the subsystem which is deep inside the bulk.

We further show that edge localization near half filling alone is not sufficient to establish topological character by explicitly analyzing domain-wall configurations in the SSH chain. In particular, we demonstrate that non-topological domain-wall states can also give rise to vanishing entanglement-entropy differences. By systematically tuning the chosen subsystem, we show that genuine topological zero-energy states remain robust exhibiting vanishing  $\Delta S_{\text{DW}}^{\mathcal{A}}$  whereas trivially localized finite energy states lose this property. This domain wall analysis establishes a systematic protocol in which entanglement entropy diagnoses localization near half filling as a necessary condition, while the topological nature is confirmed through an additional check of robustness against shrinking subsystem size.

In addition to numerical evidence, we develop a general analytic framework based on the Lyapunov exponent (LE) to determine the boundaries between topological and trivial phases. The LE is computed using the transfer matrix method. This analytical framework is straightforward and can be used to obtain the expression of boundaries in systems with complex disorders also.

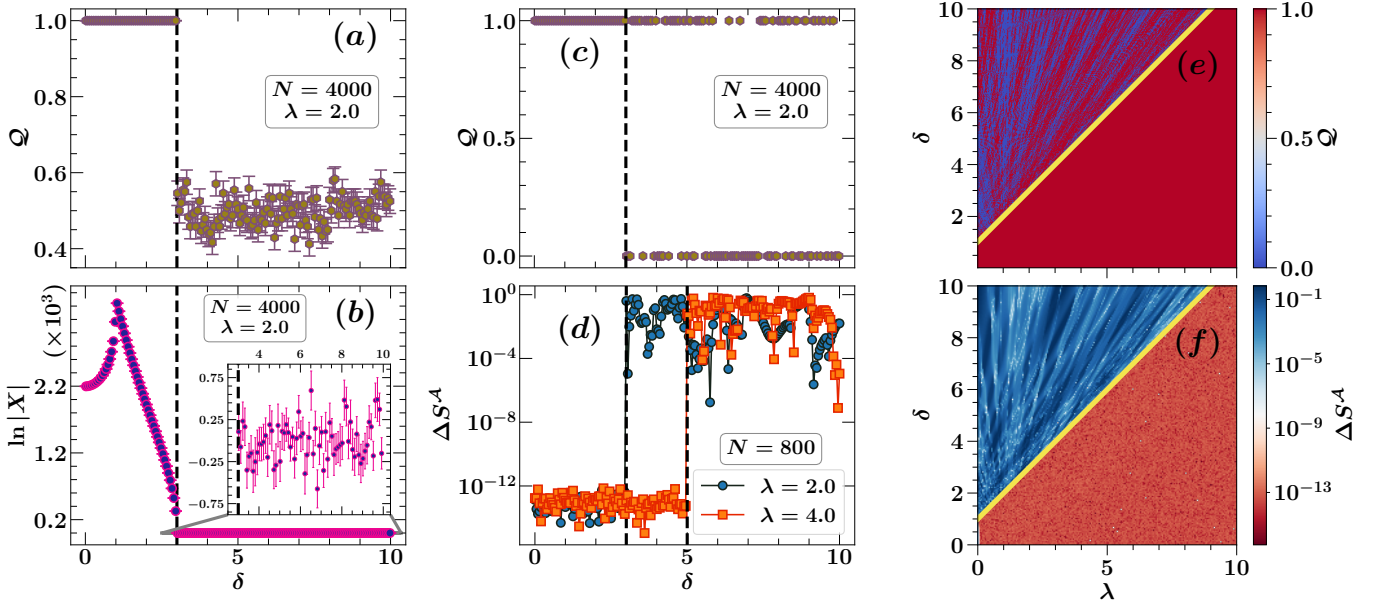


FIG. 9. Characterization of the topological phase transition and comparative reliability of diagnostics for the quasiperiodic SSH model  $t = 1$ . Panels (a)-(d) show data for a fixed  $\lambda = 2.0$  as a function of disorder strength  $\delta$ , while panels (e) and (f) present full phase diagrams in the  $\lambda$ - $\delta$  plane for a single disorder realization. (a) Topological quantum number  $Q$  ( $N = 4000$ ,  $\lambda = 2.0$ ), averaged over 480 configurations. The system transitions from the topological phase ( $Q = 1$ ) to the trivial phase ( $Q = 0$ ) near the analytical phase boundary  $\delta = t + \lambda = 3.0$  (black dashed line). In the trivial regime ( $\delta > 3.0$ ), the average value of  $Q$  converges to approximately 0.5 instead of zero, indicating a failure to clearly distinguish the phases upon averaging. (b) The behavior of  $\ln |X|$ , the underlying quantity from which  $Q$  is derived (see Eqs. (A3) and (A4)). In the topological phase,  $\ln |X| > 0$ , but in the trivial phase ( $\delta > t + \lambda$ ), it fluctuates symmetrically around zero. The inset shows a zoomed-in view of these fluctuations. These fluctuations explain the averaged value of  $Q \approx 0.5$  observed in (a), as  $Q$  takes values of 1 and 0 with roughly equal probability when  $\ln |X|$  changes sign. (c, d) Direct comparison of  $Q$  and the entanglement entropy difference  $\Delta S^A$  for a single disorder realization. (c) The value of  $Q$  can be misleadingly equal to 1 in patches deep within the trivial phase ( $\delta > 3.0$ ), indicating a lack of reliability for single configurations. (d) In contrast, the entanglement entropy difference  $\Delta S^A = |S_{hf}^A - S_{hf+1}^A|$ , calculated for a system of size  $N = 800$ , provides a sharp distinction: it remains vanishingly small ( $\sim 10^{-12}$ ) in the topological phase and rises abruptly to finite values ( $> 10^{-5}$ ) in the trivial phase. This demonstrates that  $\Delta S^A$  is a robust single-configuration diagnostic. (e, f) Phase diagrams from a single realization of quasiperiodic disorder, highlighting the contrast between the two diagnostics. (e) Phase diagram computed from  $Q$  ( $N = 4000$ ). While the topological phase ( $\delta < t + \lambda$ , red) is correctly identified,  $Q$  spuriously yields a value of 1 in numerous patches within the trivial phase ( $\delta > t + \lambda$ ), leading to a false-positive identification of topology. (f) Phase diagram computed from  $\Delta S^A$  ( $N = 800$ ). The transition is unambiguous:  $\Delta S^A$  is effectively zero (red) in the topological phase and becomes finite (blue) in the trivial phase, sharply following the analytical boundary  $\delta = t + \lambda$  (yellow line). These full phase diagrams confirm that the entanglement entropy difference is a superior and reliable metric for distinguishing topological from trivial phases, even without configuration averaging.

We find excellent agreement between our analytical predictions and numerical results across all models studied, even in the presence of disorder. Finally, we validate our conclusions using the topological quantum number  $Q$ , a known topological invariant, and find full consistency in the case of clean SSH and random binary disorder models. However, in the presence of quasiperiodic disorder in the hopping terms,  $Q$  exhibits ambiguous behavior, particularly in the trivial regime. To investigate this further, we compare  $Q$  with the EE-based diagnostic  $\Delta S^A$ , and find that the latter vanishes in the topological phase even when a single disorder realization is considered.

In this work, we establish a new quantity,  $\Delta S^A$ , which probes topological phase transitions in the 1D SSH model. While 1D systems host only two edge modes,

higher-dimensional topological insulators (e.g., 2D Chern insulators or 3D  $\mathbb{Z}_2$  topological insulators) exhibit richer edge/surface state structures. It is therefore compelling to extend this entanglement-based diagnostic to 2D and 3D systems, where the interplay between bulk topology and entanglement scaling remains incompletely explored. It is well known that topological phases are accompanied by characteristic patterns of long-range entanglement in the ground state [47]. By using entanglement entropy (a quantum-information concept) to detect topological phases (a many-body phenomenon), our work contributes to the growing field of research of unifying quantum information science and condensed matter physics. Finally, we note that the use of entanglement spectrum to diagnose topological phases has also been explored in

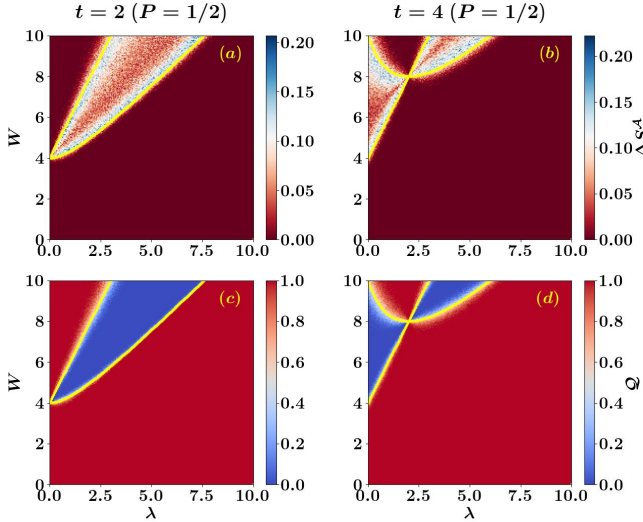


FIG. 10. Phase diagrams for the SSH model with binary disorder with probability  $P = 1/2$ . (a,b) Entanglement entropy difference  $\Delta S^A = |S_{hf}^A - S_{hf+1}^A|$  and (c,d) topological quantum number  $Q$ , plotted as functions of binary disorder strength  $W$  and dimerization  $\lambda$ . Left column (a,c):  $t = 2$ ; right column (b,d):  $t = 4$ .  $\Delta S^A$  is calculated at half filling with  $N_A = 50$ . For all figures the system size is  $N = 400$ . For all the cases, the averaging is done over 100 disorder realizations. Yellow curves denote analytical phase boundaries derived from Lyapunov exponents, separating topological (red) and trivial (blue) phases. The agreement between  $\Delta S^A$ ,  $Q$ , and analytical boundaries confirms the robustness of our approach. Red (blue) regions denote  $Q = 1$  ( $Q = 0$ ) and  $\Delta S^A = 0$  ( $\Delta S^A > 0$ ), corresponding to topological and trivial phases respectively.

earlier work by Fidkowski [56]; establishing a bridge between Fidkowski's approach and our method is desirable.

## ACKNOWLEDGMENTS

We thank Ivan M. Khaymovich for valuable discussions. We are grateful to the High Performance Computing (HPC) facility at IISER Bhopal, where some calculations in this project were run. M.K is grateful to the Council of Scientific and Industrial Research (CSIR), India, for his PhD fellowship.

## Appendix A: Topological quantum number

To support our claims obtained using the entanglement entropy, we use an established quantity, the topological quantum number  $Q$ , to distinguish a topological phase from a trivial phase, which works even in the presence of disorder. The topological quantum number is defined as

$$Q = \nu(r), \quad (A1)$$

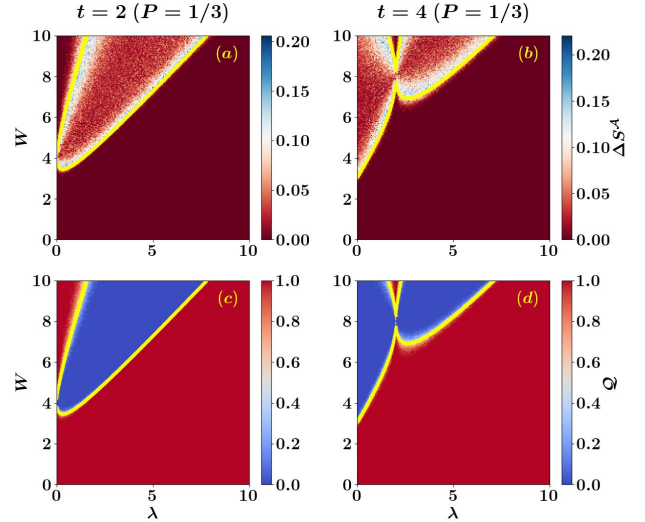


FIG. 11. Phase diagrams for the SSH model with binary disorder with probability  $P = 1/3$ . The entanglement entropy difference  $\Delta S^A$  (a,b) and the topological quantum number  $Q$  (c,d) are shown as functions of disorder strength  $W$  and dimerization  $\lambda$ . Results for two hopping strengths are presented:  $t = 2$  (left column) and  $t = 4$  (right column).  $\Delta S^A$  is calculated at half filling with  $N_A = 50$ . For all figures the system size is  $N = 400$ . Data are averaged over 100 disorder realizations. The analytically derived phase boundaries (yellow curves) excellently match with the numerical results, robustly distinguishing the topological ( $Q = 1$ ,  $\Delta S^A = 0$ ; red) and trivial ( $Q = 0$ ,  $\Delta S^A > 0$ ; blue) phases.

where  $r$  is the reflection matrix and  $\nu(r)$  denotes the number of negative eigenvalues of  $r$  [43, 44]. A negative eigenvalue of  $r$  corresponds to a phase shift of  $\pi$  in the reflected wave, indicating complete reflection due to the presence of a zero-energy boundary state [74]. For  $N_C$  coupled SSH chains,  $\nu(r) \in \{0, 1, 2, \dots, N_C\}$ , and this corresponds to the number of pairs of zero-energy edge modes.

For a single SSH chain, the reflection matrix  $r$  is a scalar and is given by

$$r = \frac{1 - X^2}{1 + X^2}, \quad (A2)$$

where

$$X = (-1)^{N/2} \prod_{n=1}^{N/2} \frac{t_{2,n}}{t_{1,n}}, \quad (A3)$$

with  $t_{1,n}$  and  $t_{2,n}$  being the intra-cell and inter-cell hoppings of the  $n^{\text{th}}$  unit cell, respectively. Hence, for a single SSH chain, the topological quantum number can be written as

$$Q = \frac{1}{2}(1 - Q'), \quad (A4)$$

where  $Q' = \text{sign}(r) \in \{-1, 1\}$ . Hence, in the trivial phase,  $Q = 0$  (no edge modes); in the topological phase,  $Q = 1$  due to one pair of zero-energy edge modes.

To corroborate the results derived from  $\Delta S^A$ , we present phase diagrams for all three models in Figs. 2(d–f). For the cases of clean SSH (Fig. 2(d)) and binary random disorder (Fig. 2(f)), our results show the expected behavior, i.e.  $\mathcal{Q} = 1$  in the topological regime and  $\mathcal{Q} = 0$  in the trivial regime. The analytically calculated boundaries, shown as yellow lines, match precisely with the numerical results. These findings are fully consistent with the observations from the entanglement entropy and further confirm that  $\Delta S^A$  is an effective measure for distinguishing topological and trivial phases.

For the case of quasiperiodic disorder, Fig. 2(e) shows that  $\mathcal{Q} = 1$  throughout the entire topological regime. However, in the trivial regime,  $\mathcal{Q}$  deviates from the expected behavior by acquiring nonzero values. Specifically, for  $\lambda = 2$ , when averaged over multiple values of  $\phi$ ,  $\mathcal{Q}$  converges to approximately 0.5 in the trivial regime (see Fig. 9(a)). To understand this average value of  $\mathcal{Q} \approx 0.5$  better, we examine the behavior of  $\mathcal{Q}' = \text{sign}(1 - X^2) = -\text{sign}(\log |X|)$ , which changes sign at the phase transition. Figure 9(b) shows that in the topological regime,  $\log |X| > 0$ , while in the trivial regime,  $\log |X|$  fluctuates around zero. This fluctuation is the origin of the average  $\mathcal{Q} \approx 0.5$ . To gain deeper insight, we next study  $\mathcal{Q}$  for a single realization.

### 1. Comparison between $\mathcal{Q}$ and $\Delta S^A$

Here, we compare the topological quantum number  $\mathcal{Q}$  with the entanglement-based quantity  $\Delta S^A$  for a single realization of the quasiperiodic phase  $\phi$ . In Fig. 9(c), we plot  $\mathcal{Q}$  as a function of  $\delta$  for  $\lambda = 2$ . While  $\mathcal{Q} = 1$  across the entire topological region ( $\delta < t + \lambda$ ), it fluctuates between 0 and 1 in the trivial regime ( $\delta > t + \lambda$ ). A similar behavior of  $\mathcal{Q}$  is visible in Fig. 9(e) for all values of  $(\delta, \lambda)$  in the interval  $[0, 10]$ . Interestingly, patches with  $\mathcal{Q} = 1$  appear even within the trivial region, which could falsely

suggest topological insulating behavior. This demonstrates that  $\mathcal{Q}$  cannot sharply identify the boundary between topological and trivial phases. In contrast, our proposed diagnostic,  $\Delta S^A$ , provides a sharp and reliable distinction between the two phases, as shown in Figs. 9(d,f).

### Appendix B: Additional results for random binary disorder case

Here, we present our numerical results for the SSH model with random binary disorder in the hopping amplitudes. We first show the plots for probability  $P = 1/2$  for various values of  $t$ . The topological phase is clearly distinguished from the trivial phase in the  $W-\lambda$  plane, as shown by the entanglement entropy difference  $\Delta S^A$  in Figs. 10(a), 10(b), and by the topological invariant  $\mathcal{Q}$  in Figs. 10(c), 10(d), thereby confirming the consistency of our numerical technique. Additionally, the yellow curves represent the analytically obtained phase boundaries, which cleanly separate the topological and trivial phases, thereby validating our analytical method.

Next, we examine the case of  $P = 1/3$ . In this scenario, the disorder  $\Delta_n$  is distributed as:

$$\Delta_n = \begin{cases} 2, & \text{with probability } 1/3, \\ 2 - W, & \text{with probability } 2/3. \end{cases} \quad (\text{B1})$$

The analytical expressions for the topological phase boundaries are obtained by substituting  $P = 1/3$  into Eq. (32) and Eq. (33). We validate these boundaries numerically using both the entanglement entropy difference  $\Delta S^A$  and the topological invariant  $\mathcal{Q}$ , as shown in Fig. 11. The excellent agreement between the analytical and numerical results further confirms the robustness of our approach.

---

[1] A. Osterloh, L. Amico, G. Falci, and R. Fazio, Scaling of entanglement close to a quantum phase transition, *Nature* **416**, 608 (2002).

[2] G. Vidal, J. I. Latorre, E. Rico, and A. Kitaev, Entanglement in quantum critical phenomena, *Phys. Rev. Lett.* **90**, 227902 (2003).

[3] T. J. Osborne and M. A. Nielsen, Entanglement in a simple quantum phase transition, *Phys. Rev. A* **66**, 032110 (2002).

[4] J. Eisert, M. Cramer, and M. B. Plenio, Colloquium: Area laws for the entanglement entropy, *Rev. Mod. Phys.* **82**, 277 (2010).

[5] C. H. Bennett, H. J. Bernstein, S. Popescu, and B. Schumacher, Concentrating partial entanglement by local operations, *Phys. Rev. A* **53**, 2046 (1996).

[6] L. D. Landau, On the theory of phase transitions, *Zh. Eksp. Teor. Fiz.* **7**, 19 (1937).

[7] A. J. Beekman, L. Rademaker, and J. van Wezel, An introduction to spontaneous symmetry breaking, *SciPost Phys. Lect. Notes*, 11 (2019).

[8] L. D. Landau, E. M. Lifshitz, E. M. Lifshits, and L. P. Pitaevskii, *Statistical Physics: Theory of the Condensed State*, Vol. 9 (Butterworth-Heinemann, London, 1980).

[9] M. Z. Hasan and C. L. Kane, Colloquium: Topological insulators, *Rev. Mod. Phys.* **82**, 3045 (2010).

[10] X.-L. Qi and S.-C. Zhang, Topological insulators and superconductors, *Rev. Mod. Phys.* **83**, 1057 (2011).

[11] J. E. Moore, The birth of topological insulators, *Nature* **464**, 194 (2010).

[12] L. Fu and C. L. Kane, Topological insulators with inversion symmetry, *Phys. Rev. B* **76**, 045302 (2007).

[13] B. A. Bernevig, *Topological Insulators and Topological Superconductors* (Princeton University Press, Princeton, 2013).

[14] J. K. Asbóth, L. Oroszlány, and A. Pályi, *A Short Course on Topological Insulators* (Springer International Pub-

lishing, 2016).

[15] K. v. Klitzing, G. Dorda, and M. Pepper, New method for high-accuracy determination of the fine-structure constant based on quantized hall resistance, *Phys. Rev. Lett.* **45**, 494 (1980).

[16] J. E. Moore and L. Balents, Topological invariants of time-reversal-invariant band structures, *Phys. Rev. B* **75**, 121306 (2007).

[17] D. N. Sheng, Z. Y. Weng, L. Sheng, and F. D. M. Haldane, Quantum spin-hall effect and topologically invariant chern numbers, *Phys. Rev. Lett.* **97**, 036808 (2006).

[18] T. Fukui and Y. Hatsugai, Topological aspects of the quantum spin-hall effect in graphene:  $Z_2$  topological order and spin chern number, *Phys. Rev. B* **75**, 121403 (2007).

[19] C. L. Kane and E. J. Mele,  $Z_2$  topological order and the quantum spin hall effect, *Phys. Rev. Lett.* **95**, 146802 (2005).

[20] L. Fu and C. L. Kane, Time reversal polarization and a  $Z_2$  adiabatic spin pump, *Phys. Rev. B* **74**, 195312 (2006).

[21] R. Roy,  $Z_2$  classification of quantum spin hall systems: An approach using time-reversal invariance, *Phys. Rev. B* **79**, 195321 (2009).

[22] E. Prodan, Robustness of the spin-chern number, *Phys. Rev. B* **80**, 125327 (2009).

[23] B. Leung and E. Prodan, Effect of strong disorder in a three-dimensional topological insulator: Phase diagram and maps of the  $F_2$  invariant, *Phys. Rev. B* **85**, 205136 (2012).

[24] Z. Wang and S.-C. Zhang, Simplified topological invariants for interacting insulators, *Phys. Rev. X* **2**, 031008 (2012).

[25] B. Pérez-González, M. Bello, A. Gómez-León, and G. Platero, Interplay between long-range hopping and disorder in topological systems, *Phys. Rev. B* **99**, 035146 (2019).

[26] L. Li and S. Chen, Characterization of topological phase transitions via topological properties of transition points, *Phys. Rev. B* **92**, 085118 (2015).

[27] C.-K. Chiu, J. C. Y. Teo, A. P. Schnyder, and S. Ryu, Classification of topological quantum matter with symmetries, *Rev. Mod. Phys.* **88**, 035005 (2016).

[28] X.-G. Wen, Colloquium: Zoo of quantum-topological phases of matter, *Rev. Mod. Phys.* **89**, 041004 (2017).

[29] B. J. Wieder, B. Bradlyn, J. Cano, Z. Wang, M. G. Vergniory, L. Elcoro, A. A. Soluyanov, C. Felser, T. Neupert, N. Regnault, and B. A. Bernevig, Topological materials discovery from crystal symmetry, *Nature Reviews Materials* **7**, 196 (2022).

[30] K. L. Hur, L. Henriet, A. Petrescu, K. Plekhanov, G. Roux, and M. Schiró, Many-body quantum electrodynamics networks: Non-equilibrium condensed matter physics with light, *Comptes Rendus. Physique* **17**, 808 (2016).

[31] L. Lu, J. D. Joannopoulos, and M. Soljačić, Topological photonics, *Nature Photonics* **8**, 821 (2014).

[32] T. Ozawa, H. M. Price, A. Amo, N. Goldman, M. Hafezi, L. Lu, M. C. Rechtsman, D. Schuster, J. Simon, O. Zilberman, and I. Carusotto, Topological photonics, *Rev. Mod. Phys.* **91**, 015006 (2019).

[33] D. Zhang, M. Long, L. Cui, J. Xiao, and C. Pan, Perfect spin-filtering and switching functions in zigzag silicene nanoribbons with hydrogen modification, *Organic Electronics* **62**, 253 (2018).

[34] V. Galitski and I. B. Spielman, Spin-orbit coupling in quantum gases, *Nature* **494**, 49 (2013).

[35] N. R. Cooper, J. Dalibard, and I. B. Spielman, Topological bands for ultracold atoms, *Rev. Mod. Phys.* **91**, 015005 (2019).

[36] N. Goldman, J. C. Budich, and P. Zoller, Topological quantum matter with ultracold gases in optical lattices, *Nature Physics* **12**, 639 (2016).

[37] G. Vidal, Efficient classical simulation of slightly entangled quantum computations, *Phys. Rev. Lett.* **91**, 147902 (2003).

[38] R. Pawlak, S. Hoffman, J. Klinovaja, D. Loss, and E. Meyer, Majorana fermions in magnetic chains, *Progress in Particle and Nuclear Physics* **107**, 1 (2019).

[39] L. Li, C. Yang, and S. Chen, Winding numbers of phase transition points for one-dimensional topological systems, *Europhysics Letters* **112**, 10004 (2015).

[40] R. K. Malakar and A. K. Ghosh, Engineering topological phases of any winding and chern numbers in extended su-schrieffer-heeger models, *Journal of Physics: Condensed Matter* **35**, 335401 (2023).

[41] M. G. Yamada, Topological  $Z_2$  invariant in kitaev spin liquids: Classification of gapped spin liquids beyond projective symmetry group, *Phys. Rev. Res.* **3**, L012001 (2021).

[42] I. Mondragon-Shem, T. L. Hughes, J. Song, and E. Prodan, Topological criticality in the chiral-symmetric aiii class at strong disorder, *Phys. Rev. Lett.* **113**, 046802 (2014).

[43] I. C. Fulga, F. Hassler, A. R. Akhmerov, and C. W. J. Beenakker, Scattering formula for the topological quantum number of a disordered multimode wire, *Phys. Rev. B* **83**, 155429 (2011).

[44] P. Zhang and F. Nori, Majorana bound states in a disordered quantum dot chain, *New Journal of Physics* **18**, 043033 (2016).

[45] N. Ahmadi, J. Abouie, and D. Baeriswyl, Topological and nontopological features of generalized su-schrieffer-heeger models, *Phys. Rev. B* **101**, 195117 (2020).

[46] R. Nehra, D. S. Bhakuni, S. Gangadharaiah, and A. Sharma, Many-body entanglement in a topological chiral ladder, *Phys. Rev. B* **98**, 045120 (2018).

[47] B. Zeng, X. Chen, D.-L. Zhou, and X.-G. Wen, *Quantum information meets quantum matter – from quantum entanglement to topological phase in many-body systems* (2018), arXiv:1508.02595 [cond-mat.str-el].

[48] A. Hamma, W. Zhang, S. Haas, and D. A. Lidar, Entanglement, fidelity, and topological entropy in a quantum phase transition to topological order, *Phys. Rev. B* **77**, 155111 (2008).

[49] T. P. Oliveira and P. D. Sacramento, Entanglement modes and topological phase transitions in superconductors, *Phys. Rev. B* **89**, 094512 (2014).

[50] H.-C. Jiang, Z. Wang, and L. Balents, Identifying topological order by entanglement entropy, *Nature Physics* **8**, 902 (2012).

[51] T. Maslowski and N. Sedlmayr, Quasiperiodic dynamical quantum phase transitions in multiband topological insulators and connections with entanglement entropy and fidelity susceptibility, *Phys. Rev. B* **101**, 014301 (2020).

[52] C. Castelnovo and C. Chamon, Quantum topological phase transition at the microscopic level, *Phys. Rev. B* **77**, 054433 (2008).

[53] T. Grover, A. M. Turner, and A. Vishwanath, Entangle-

ment entropy of gapped phases and topological order in three dimensions, *Phys. Rev. B* **84**, 195120 (2011).

[54] A. M. Turner, F. Pollmann, and E. Berg, Topological phases of one-dimensional fermions: An entanglement point of view, *Phys. Rev. B* **83**, 075102 (2011).

[55] F. Pollmann, A. M. Turner, E. Berg, and M. Oshikawa, Entanglement spectrum of a topological phase in one dimension, *Phys. Rev. B* **81**, 064439 (2010).

[56] L. Fidkowski, Entanglement spectrum of topological insulators and superconductors, *Phys. Rev. Lett.* **104**, 130502 (2010).

[57] W. P. Su, J. R. Schrieffer, and A. J. Heeger, Solitons in polyacetylene, *Phys. Rev. Lett.* **42**, 1698 (1979).

[58] W. P. Su, J. R. Schrieffer, and A. J. Heeger, Soliton excitations in polyacetylene, *Phys. Rev. B* **22**, 2099 (1980).

[59] L. Li, Z. Xu, and S. Chen, Topological phases of generalized su-schrieffer-heeger models, *Phys. Rev. B* **89**, 085111 (2014).

[60] T. Liu and H. Guo, Topological phase transition in the quasiperiodic disordered su-schrieffer-heeger chain, *Physics Letters A* **382**, 3287 (2018).

[61] A. Sinha, T. Shit, A. Tatarwal, D. Sen, and S. Mukherjee, Probing the topological anderson transition in quasiperiodic photonic lattices via chiral displacement and wavelength tuning, *Phys. Rev. A* **112**, 013512 (2025).

[62] S.-N. Liu, G.-Q. Zhang, L.-Z. Tang, and D.-W. Zhang, Topological anderson insulators induced by random binary disorders, *Physics Letters A* **431**, 128004 (2022).

[63] S. Mandal and S. Kar, Topological solitons in a su-schrieffer-heeger chain with periodic hopping modulation, domain wall, and disorder, *Phys. Rev. B* **109**, 195124 (2024).

[64] L.-Z. Tang, S.-N. Liu, G.-Q. Zhang, and D.-W. Zhang, Topological anderson insulators with different bulk states in quasiperiodic chains, *Phys. Rev. A* **105**, 063327 (2022).

[65] X. Li, H. Xu, J. Wang, L.-Z. Tang, D.-W. Zhang, C. Yang, T. Su, C. Wang, Z. Mi, W. Sun, X. Liang, M. Chen, C. Li, Y. Zhang, K. Linghu, J. Han, W. Liu, Y. Feng, P. Liu, G. Xue, J. Zhang, Y. Jin, S.-L. Zhu, H. Yu, S. P. Zhao, and Q.-K. Xue, Mapping the topology-localization phase diagram with quasiperiodic disorder using a programmable superconducting simulator, *Phys. Rev. Res.* **6**, L042038 (2024).

[66] S. Li, M. Liu, F. Li, and B. Liu, Topological phase transition of the extended non-hermitian su-schrieffer-heeger model, *Physica Scripta* **96**, 015402 (2020).

[67] A. Nava, G. Campagnano, P. Sodano, and D. Giuliano, Lindblad master equation approach to the topological phase transition in the disordered su-schrieffer-heeger model, *Phys. Rev. B* **107**, 035113 (2023).

[68] Z.-S. Xu, J. Gao, A. Iovan, I. M. Khaymovich, V. Zwiller, and A. W. Elshaari, Observation of reentrant metal-insulator transition in a random-dimer disordered ssh lattice, *npj Nanophotonics* **1**, 8 (2024).

[69] Y. Wang, X. Xia, L. Zhang, H. Yao, S. Chen, J. You, Q. Zhou, and X.-J. Liu, One-dimensional quasiperiodic mosaic lattice with exact mobility edges, *Phys. Rev. Lett.* **125**, 196604 (2020).

[70] X. Cai and Y.-C. Yu, Exact mobility edges in quasiperiodic systems without self-duality, *Journal of Physics: Condensed Matter* **35**, 035602 (2022).

[71] X.-C. Zhou, Y. Wang, T.-F. J. Poon, Q. Zhou, and X.-J. Liu, Exact new mobility edges between critical and localized states, *Phys. Rev. Lett.* **131**, 176401 (2023).

[72] Z. Wang, Y. Zhang, L. Wang, and S. Chen, Engineering mobility in quasiperiodic lattices with exact mobility edges, *Phys. Rev. B* **108**, 174202 (2023).

[73] Y. Wang, X. Xia, Y. Wang, Z. Zheng, and X.-J. Liu, Duality between two generalized aubry-andré models with exact mobility edges, *Phys. Rev. B* **103**, 174205 (2021).

[74] A. R. Akhmerov, J. P. Dahlhaus, F. Hassler, M. Wimmer, and C. W. J. Beenakker, Quantized conductance at the majorana phase transition in a disordered superconducting wire, *Phys. Rev. Lett.* **106**, 057001 (2011).

[75] H. Weyl, Über die gleichverteilung von zahlen mod. eins, *Mathematische Annalen* **77**, 313 (1916).

[76] G. H. Choe, Ergodicity and irrational rotations, *Proceedings of the Royal Irish Academy. Section A: Mathematical and Physical Sciences* **93A**, 193 (1993).

[77] S. Longhi, Metal-insulator phase transition in a non-hermitian aubry-andré-harper model, *Phys. Rev. B* **100**, 125157 (2019).

[78] I. S. Gradshteyn and I. M. Ryzhik, *Table of Integrals, Series, and Products*, seventh ed., edited by D. Zwillinger (Academic Press, Amsterdam, 2007).

[79] I. Peschel, Calculation of reduced density matrices from correlation functions, *Journal of Physics A: Mathematical and General* **36**, L205 (2003).

[80] I. Peschel and V. Eisler, Reduced density matrices and entanglement entropy in free lattice models, *Journal of Physics A: Mathematical and Theoretical* **42**, 504003 (2009).

[81] I. Peschel, Special review: Entanglement in solvable many-particle models, *Brazilian Journal of Physics* **42**, 267 (2012).

[82] S. Aubry and G. André, Analyticity breaking and anderson localization in incommensurate lattices, *Ann. Isr. Phys. Soc.* **3**, 133 (1980).

[83] N. Roy and A. Sharma, Study of counterintuitive transport properties in the aubry-andré-harper model via entanglement entropy and persistent current, *Phys. Rev. B* **100**, 195143 (2019).

[84] D. Sahu, V. Khade, and S. Gangadharaiah, Effect of topological length on bound state signatures in a topological nanowire, *Phys. Rev. B* **108**, 205426 (2023).

[85] F. Munoz, F. Pinilla, J. Mella, and M. I. Molina, Topological properties of a bipartite lattice of domain wall states, *Scientific Reports* **8**, 17330 (2018).